CTU Journal of Innovation and Sustainable Development
ISSN 2588-1418 | e-ISSN 2815-6412

DOI:10.22144/ctujoisd.2026.015

Investigation of optical properties of Mn^{4+} doped $ZnAl_2O_4$ phosphor fabricated by sol-gel method

Ly Trieu Loc[1], Tran Thi Thuy Tien[1], Lam Tan Phat[1], Nguyen Tran Yen Vy[1], To Vo Hoai Phong[1], Nguyen Thi Kim Chi[2], and Dinh Manh Tien[3,4*]

[1]*Students of Engineering Physics, College of Natural Science, Can Tho University, Viet Nam*

[2]*College of Natural Science, Can Tho University, Viet Nam*

[3]*College of Engineering, Can Tho University, Viet Nam*

[4]*School of Materials, HaNoi University of Science and Technology, Viet Nam*

**Corresponding author (dmtien@ctu.edu.vn)*

Article info.

Received 12 May 2025
Revised 30 May 2025
Accepted 30 Jan 2026

Keywords

Sol-gel method, red emission, transition metal ions, WLED, $ZnAl_2O_4$: Mn^{4+}

ABSTRACT

In this work, $ZnAl_2O_4$: Mn^{4+} phosphor is prepared by the sol-gel method. The phase structure was investigated by X-ray diffraction (XRD), and morphology and element composition were analysed by scanning electron microscopy (SEM), energy-dispersive X-ray spectroscopy (EDX), luminescent performance of the phosphor using photoluminescence (PL) spectra, and Raman spectroscopy. The obtained powder shows a red broad emission band peaking at 676 nm and 692 nm, corresponding to the energy transfer of electrons from ^2E_g to $^4A_{2g}$. The Mn^{4+} concentration is doped at 0.5 mol% into the $ZnAl_2O_4$ host lattice. After that, the powder annealed at 1200°C for 4 hours in the air revealed an average crystallite size of about 52.833 nm and a high emission intensity with (x, y) CIE colour coordinates (0.2705, 0.2741). Therefore, $ZnAl_2O_4$: Mn^{4+} phosphor could be a promising material for solid-state lighting applications.

1. INTRODUCTION

Solid State Lighting (SSL) has recently held an essential societal position. With outstanding advantages in aesthetics, convenience, luminous efficacy, and various types and colours, LED (Light Emitting Diode) technology has gradually replaced traditional lighting systems such as arc lamp or incandescent light bulb. According to Elliott et al. (2020), LED products accounted for approximately 30% of all lighting installations in the USA (United States of America) by the end of 2018, helping save about 1.3 quadrillion BTUs (British Thermal Units) annually. In their reports, Khan et al. (2011) and Liu et al. (2024) show that LED has a longer lifespan than other lights used for their comparative report, low maintenance costs, and high lighting quality, especially environmentally friendly.

WLED (White Light Emitting Diode) is a type of LED, which can be fabricated in several ways, one standard method being the combination of three bare colour chips like red, green and blue (RGB), but a more common way involves using blue or UV (Ultraviolet) LED coated with yellow-emitting phosphor, which is YAG: Ce^{3+}. However, these systems often do not have enough red light components, resulting in low CRI (Colour Rendering Index) from 65 to 70 and high CCT (Correlated Colour Temperature). In some cases, it produces light that isn't eye-friendly. Many solutions have been mentioned. Yadav et al. (2018) report on the synthesis material YAG: Ce^{3+} but

replace Ce^{3+} with Gd^{3+}, Pr^{3+}, or Tb^{3+} to help improve CRI. Jiang et al. (2018) used a combination of Mg^{2+} and Ge^{4+} to partially replace Al^{3+}; the results show that CCT decreases from 6798K to 3261K and CRI increases from 76.5 to 89.3. In addition, Ma et al. (2020) have announced that the CRI result is 84.8 when they co-doped Pr^{3+} and Mn^{2+} into YAG: Ce^{3+} transparent ceramics, and Li et al. (2023) have also reported on doping Cr^{3+} to improve red light components with YAG: Ce^{3+}.

Spinel structure materials, with the general formula AB_2O_4, where A = Mg, Ca, Zn, and B = Ti, Ga, Al, are dielectric compounds characterised by a wide band gap (López et al., 2009). According to Di Quarto et al. (2023), its band gap ranges from 1 eV $< E_g <$ 8 eV, depending on the nature of the A and B metal cations. Martins et al. (2010) indicated that the energy gap between the valence and conduction bands corresponds to ultraviolet photon emission, so these spinels are transparent and non-absorptive across the visible spectrum. Numerous studies have explored the use of AB_2O_4 spinel structure as host matrices. Results show that doping these spinels with transition-metal or rare-earth ions yields materials with high luminescent efficiency, excellent chemical and mechanical stability, and thermal resistance, making spinels promising candidates for modern technological applications. For example, based on previous research, Kuma et al. (2007) developed $ZnAl_2O_4$ thin films to explore their potential in electronics and optics. Nuryadin et al. (2017) synthesised and studied $ZnAl_2O_4$: Mn^{4+} and realised potential photocatalytic activity, suitable for pollutant degradation processes. Additionally, the synthesis of SrY_2O_4 spinel and the result that SrY_2O_4 has high luminescence efficiency suggest its potential use in field emission display technologies (Priya et al., 2020).

Zinc aluminate ($ZnAl_2O_4$) spinel structure is a well-known dielectric material with a wide optical bandgap of 3.8 eV. The result shows that zinc aluminate is transparent at wavelengths longer than 320 nm (Wu et al., 2005; Zhang et al., 2012). Zinc aluminate spinel is one of the important host lattices to fabricate phosphor materials because it has low cost, high durability, and the ability to be made quickly in the lab. Moreover, $ZnAl_2O_4$ spinel also has an excellent luminescence efficiency upon doping with rare-earth (RE) or transition metal ions. For its outstanding properties, this type of material has been used in many fields, such as high-temperature-resistant materials, photoelectric, electronic, and optical materials, and catalysts (Guilhaume & Primet, 1994; Wu et al., 2005). $ZnAl_2O_4$ is commonly used as a host matrix for rare-earth doped phosphor materials such as Europium (Eu), Samarium (Sm), Terbium (Tb), Cerium (Ce), and Dysprosium (Dy) doped into the $ZnAl_2O_4$ lattice have been reported and found in the literatures (He et al., 2018; Mekprasart et al., 2018; Balakrishnan et al., 2024).

Mn-doped $ZnAl_2O_4$ phosphors have been successfully studied by using different preparation methods. The synthesis of $ZnAl_2O_4$: Mn^{4+} has been reported previously by Nuryadin et al. (2017) and Vikas et al. (2025). The results show that the emitted light consists of components in the red to far-red spectral range synthesized $ZnAl_{2-x}O_4$: xMn^{4+}, x = 1 mol% by the co-precipitation method (Nuryadin et al., 2017). The sample $ZnAl_2O_4$: xMn^{4+} was prepared using the microwave combustion and then heat-treated at 900°C (Vikas et al., 2025). However, in previous studies, the focus has primarily been on doping rare-earth metal ions into the $ZnAl_2O_4$ host lattice, with limited attention to transition-metal ions. Furthermore, research on the application of Mn-doped ZnAl2O4 materials in solid-state lighting remains scarce. For these reasons, in this paper, Mn^{4+} ions doped $ZnAl_2O_4$ phosphor was chosen as the primary material and prepared using the sol-gel method. The goal is to study its light-emitting properties and see its suitability for solid-state lighting.

2. MATERIALS AND METHOD

2.1. Material

$ZnAl_2O_4$: Mn^{4+} phosphors were fabricated by the sol-gel method, as shown in Figure 1. The chemicals used in this study include: $Al(NO_3)_3.9H_2O$ – China, 98% purity, $Zn(NO_3)_2.6H_2O$ – China, 98% purity, $Mn(NO_3)_2.6H_2O$ – Merck, 48-52% and ammonia NH_3 solution.

2.2. Process preparation

The process synthesis of $ZnAl_2O_4$: Mn^{4+} phosphors was done in the laboratory, as shown in Figure 1a. Firstly, 14.9677 (g) $Al(NO_3)_3.9H_2O$ and 5.9498 (g) $Zn(NO_3)_2.6H_2O$ were placed inside some glass beakers. Subsequently, 50 ml of deionised water was added to each beaker to dissolve the $Al(NO_3)_3$ and $Zn(NO_3)_2$. Then, the mixture was magnetically stirred at 1500 rpm for 30 minutes at room temperature to obtain a well-dispersed solution. The next step was to diffuse the different amounts of Mn^{4+} ions into the $ZnAl_2O_4$ host lattice by slowly dropping 23 µL of the 50% $Mn(NO_3)_2.6H_2O$

solution into glass beakers containing $Al(NO_3)_3$ mixtures using a micropipette, followed by a process of magnetic stirring for 30 minutes at room temperature. Then, white colour precipitation $Al(OH)_3$ and $Mn(OH)_2$ crystals were obtained by adding NH3 solution to previous solutions, following this reaction:

$$3NH_3 + Al(NO_3)_3 + 3H_2O \rightarrow 3NH_4NO_3 + Al(OH)_3$$

$$2NH_3 + Mn(NO_3)_2 + 2H_2O \rightarrow 2NH_4NO_3 + Mn(OH)_2$$

The solutions were then centrifuged for 15 minutes to obtain the white gel. The as-received product was dried in an oven at 200°C for 2 hours to obtain Al_2O_3 and MnO powder through the following hydrolysis process:

$$2Al(OH)_3 \downarrow \rightarrow Al_2O_3 + 3H_2O$$

$$MN(OH)_2 \downarrow \rightarrow MnO + H_2O$$

Finally, the dried powder was finely milled and subsequently annealed in air at various temperatures to facilitate the diffusion of Mn^{4+} ions into the surface layer of the $ZnAl_2O_4$ particles.

The heating program was desbribed described in Figure 1b first, the sample was heated from room temperature (27°C) to 600°C at a rate of 5°C/min and held for 30 minutes; second, it was heated to the target annealing temperature (900–1200°C) at the same rate of 5°C/min; finally, the sample was held at the target temperature for 4 hours before natural cooling.

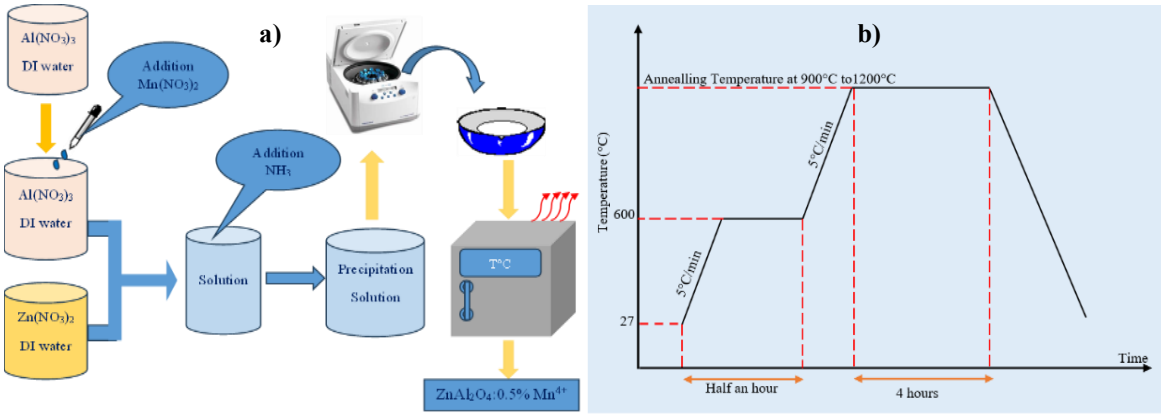

Figure 1. a) Schematic diagram of the sol-gel method process of synthesis of $ZnAl_2O_4$, b) Annealing setting programme

2.3. Characterization

The crystallinity phase structure was characterised using an X-ray diffraction instrument (XRD-D2 phaser) with a CuKa (λ = 1.5406 Å) radiation source. X'Pert HighScore Plus (Malvern Panalytical) software was utilised for analysing the XRD patterns of the synthesised $ZnAl_2O_4$: Mn^{4+} phosphors. This software facilitates phase identification and quantitative phase analysis via Rietveld refinement. The surface morphology and element composition were investigated using the emission scanning microscopy (SEM-JSM-IT200) equipment with an energy-dispersive X-ray spectroscopy (EDX). Raman microscopy was analysed using an XploRA Plus instrument (Horiba, France) with a laser source of 532 nm wavelength. The photoluminescence (PL) spectra were measured using a Nanolog spectrophotometer (Horiba). The optical properties of LED devices were studied using an integrating sphere and a HAAS spectroradiometer at Dien Quang Lamp Joint Stock Company.

3. RESULTS AND DISCUSSION

3.1. X-ray diffraction

Figure 2a shows the XRD patterns of 0.5 mol% Mn-doped $ZnAl_2O_4$ annealed at temperatures from 900°C to 1200°C for 4 hours and pure $ZnAl_2O_4$. All of the samples'XRD patterns have the characteristic diffraction peaks for phase crystallinity of $ZnAl_2O_4$ at 2θ (degree) are 31.63°, 37.19°, 45.15°, 49.42°, 55.98°, 59.67°, 65.54°, 74.63°, and 77.85°, corresponding to the (220), (113), (400), (331), (422), (511), (440), (602) and (533) phanes of the cubic gahnite structured of $ZnAl_2O_4$ phase (Fd3m space group, no. 227) were referred to ICDD 01-073-1961 (Zhu et al., 2021; Vikas et al., 2023). Additionally, Figure 2a also demonstrates that at annealing temperatures of 900°C and 1000°C, the XRD patterns of the 0.5 mol% Mn^{4+}-doped $ZnAl_2O_4$

powders show no additional peaks related to precursor metals, indicating the preservation of the cubic phase of $ZnAl_2O_4$ without the formation of impurity phases. However, when the annealing temperature was increased to 1100°C and 1200°C, in addition to the $ZnAl_2O_4$ peaks, several weaker diffraction peaks were observed, which can be attributed to the hexagonal phase of Al_2O_3, at the 2θ (degree) angles of 25.95°, 35.51°, 38.14°, 43.71°, 52.90°, 57.84°, 66.85°, and 68.53°, corresponding to the (012), (104), (110), (113), (024), (116), (214), and (300) phanes respectively of hexagonal structured Al_2O_3 (R3-c space group, no. 167) were referred to ICDD 00-048-0366. This XRD result is most likely the result of (Cornu et al., 2014).

Figure 2b shows the exaggerated XRD pattern, focused on the (220) plane, for the pure $ZnAl_2O_4$ and 0.5 mol% Mn-doped $ZnAl_2O_4$ samples annealed from 900°C to 1200°C for 4 hours. At 900°C and 1000°C of $ZnAl_2O_4$: 0.5 mol% Mn^{4+}, the diffraction peak shifts to a more extended angle than pure $ZnAl_2O_4$. These could be explained by the diffusion of Mn^{4+} ions into the $ZnAl_2O_4$ host lattice because the ionic radius of Mn^{4+} ions is 0.53 Å, smaller than that of Al^{3+} ions, which is 0.535 Å. Nevertheless, at higher temperatures, 1100°C and 1200°C, the peak shifts to a smaller angle because the samples were annealed at high temperatures, which could lead to good crystallinity and precise phase formation of Al_2O_3.

It has been reported that the lattice parameters (a, b, c), the unit cell volume (V), and the average crystallite size of $ZnAl_2O_4$ doped with Mn^{4+} ions can be derived from XRD patterns. The crystallite size calculated by Scherrer's equation (Zhang et al., 2018):

$$D = \frac{k\lambda}{\beta \cos\theta} \quad (1)$$

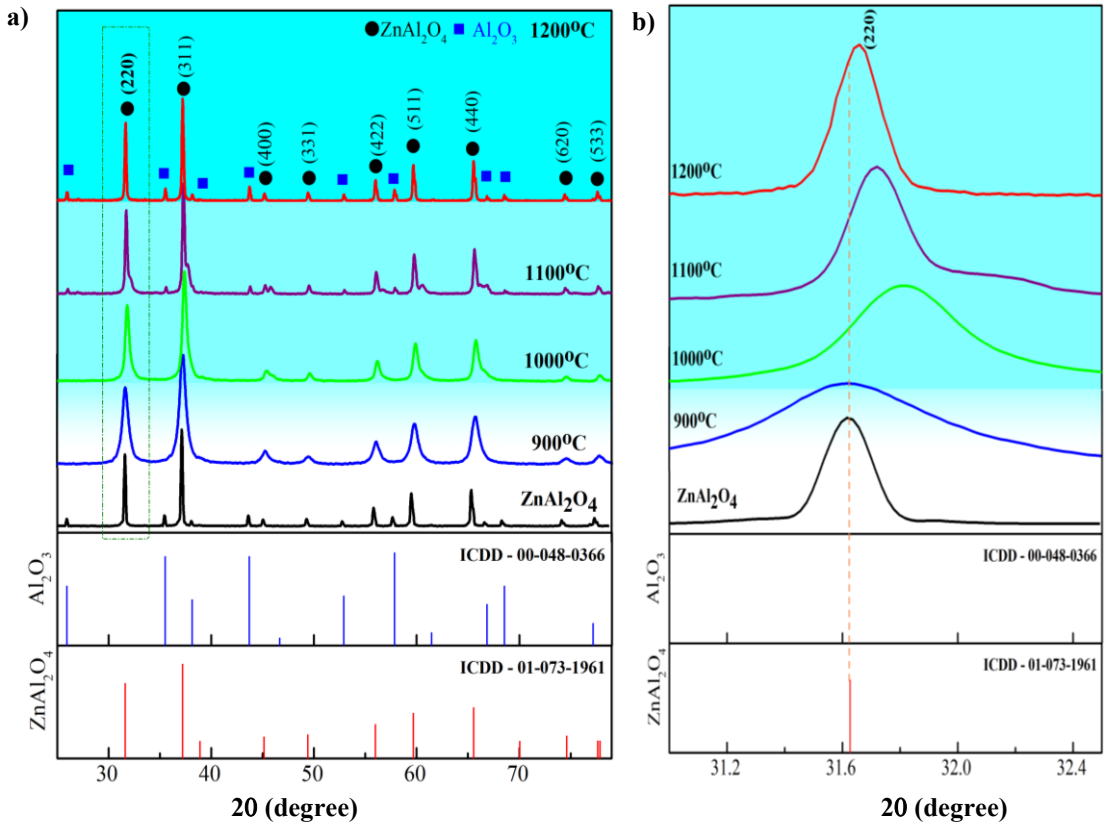

Figure 2. a) XRD patterns of pure $ZnAl_2O_4$ and $ZnAl_2O_4$: 0.5 mol% Mn^{4+} samples at the various temperatures from 900°C to 1200°C for 4 hours, and b) view of exaggerated XRD pattern at (220) plane

Where D is the crystal, λ is the wavelength of X-ray, β is the entire width of half maximum, k is the shape factor (k = 0.9), and θ is Bragg's angle. The structural constants of $ZnAl_2O_4$: 0.5 mol% Mn^{4+}

phosphor annealed from 900°C to 1200°C have successfully been calculated in detail and are listed in Table 1. The structural constants of $ZnAl_2O_4$: 0.5 mol% Mn^{4+} phosphor annealed from 900°C to 1200°C, as shown in Table 1, reveal that increasing temperature then unit cell volume and the average crystallite size also rise from 900°C to 1200°C, these results indicate the good consistency with the previous report (Cornu et al., 2014). When Mn^{4+} is doped into $ZnAl_2O_4$, the average size is 52.833 nm, annealing at 1200°C for 4 hours in the air. However, the lattice strain tends to decrease as the annealing temperature increases.

Table 1. The structure parameter of pure $ZnAl_2O_4$ and $ZnAl_2O_4$: 0.5 mol% Mn^{4+} phosphors annealed at various temperatures derived from XRD patterns

Samples	Lattice parameters *a=b=c* (Å)	Unit of volume *V* (Å^3)	Lattice strain *ε* (%)	The average crystallite size D (nm)
Pure $ZnAl_2O_4$ - 1200°C	8.0164	515.162	0.175	54.617
$ZnAl_2O_4$: 0.5 mol% Mn^{4+}-900°C	8.0111	514.134	0.496	16.867
$ZnAl_2O_4$: 0.5 mol% Mn^{4+}-1000°C	8.0114	514.192	0.345	24.144
$ZnAl_2O_4$: 0.5 mol% Mn^{4+}-1100°C	8.0263	517.066	0.295	34.289
$ZnAl_2O_4$: 0.5 mol% Mn^{4+}-1200°C	8.0368	519.098	0.187	52.833

3.2. Rietveld refinement

Figure 3. Show the phases component of the $ZnAl_2O_4$: 0.5 mol% Mn^{4+} phosphors annealed from 900°C to 1200°C for 4 hours using X'pert Highscore Plus software. The results indicate that the phase component exists in the samples. Almost, $ZnAl_2O_4$: 0.5 mol% Mn^{4+} annealed at 900°C and 1000°C have only one phase of $ZnAl_2O_4$ and no additional phases (Figure 3a, b). However, there is new phase formation at higher temperatures, 1100°C and 1200°C, there is new phase formation. They are the hexagonal phases of Al_2O_3 (Figures 3c, 3d).

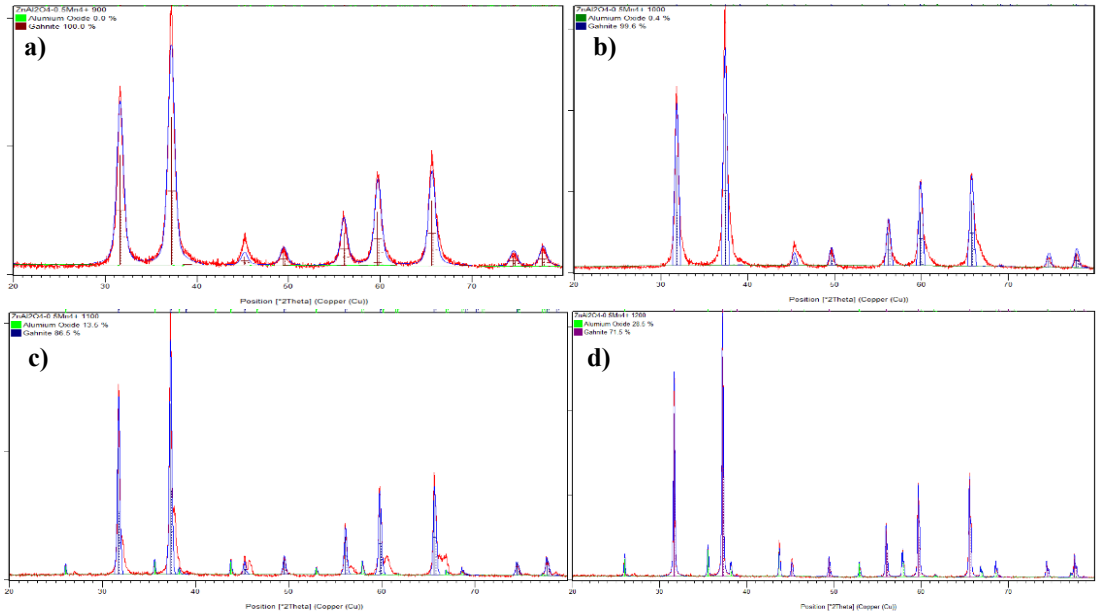

Figure 3. The phase component of the $ZnAl_2O_4$: 0.5 mol% Mn^{4+} phosphors annealed at a) 900°C, b) 1000°C, c) 1100°C and d) 1200°C

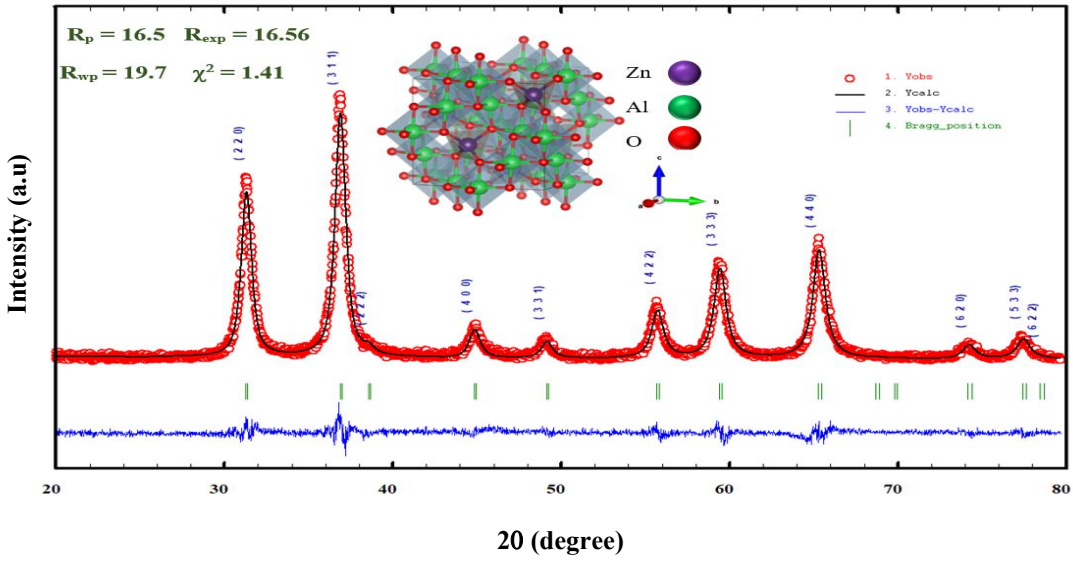

Figure 4. Rietveld refinement of the $ZnAl_2O_4$: 0.5 mol% Mn^{4+} phosphors

Figure 4 presents the Rietveld refinement of the $ZnAl_2O_4$: 0.5 mol% Mn^{4+} phosphor annealed using FullProf software. It is renowned that the refined spectrum shows good consistency with the experimental data.

The R_p, R_{exp}, R_{wp}, and chi-squared (χ^2) parameters are also shown in Figure 4, with the low value χ^2 = 1.41 illustrating the refined model's high reliability for the Rietveld investigation. This result coincides with the other reports (John & John, 2023; Vikas et al., 2023).

3.3. SEM and EDX analysis

Figure 5a-d shows the SEM images of the $ZnAl_2O_4$: 0.5 mol% Mn^{4+} powders annealed at 900 -1200°C. It has been observed that the particle size increases with increasing annealing temperature. The average particle diameter size of the $ZnAl_2O_4$: 0.5 mol% Mn^{4+} samples was 5 - 20 µm at 900°C (Figure 5a), 5 - 35 µm at 1000°C (Figure 5 b), 10 - 40 µm at 1100°C (Figure 5c), and 20 -70 µm at 1200°C (Figure 5d). The particle size increases at the high annealing temperature of 1200°C, as shown in Figure 5d. This could be explained by the accumulation of Al_2O_3 crystals on the $ZnAl_2O_4$ surface.

The EDX measurements shown in Figure 5e show that the EDX of the $ZnAl_2O_4$ powder has only three chemical elements without any other foreign elements, demonstrating the high purity of the obtained $ZnAl_2O_4$ powder. The atomic percentages shown in Figure 5e correspond to the Zn, Al, and O elements, which are 15.75, 30.19, and 54.05, respectively. Figure 5f shows the particle size distribution of $ZnAl_2O_4$: 0.5 mol% Mn^{4+} annealed at 1200°C. The size distribution chart of the obtained $ZnAl_2O_4$ particles indicates that their average size is 30–35 µm. The absence of Mn peaks in the EDX spectrum can be attributed to the low doping concentration of Mn^{4+} ions in the $ZnAl_2O_4$ lattice. Specifically, the Mn doping level is 0.5 mol%, which may be below the detection limit of the EDX technique.

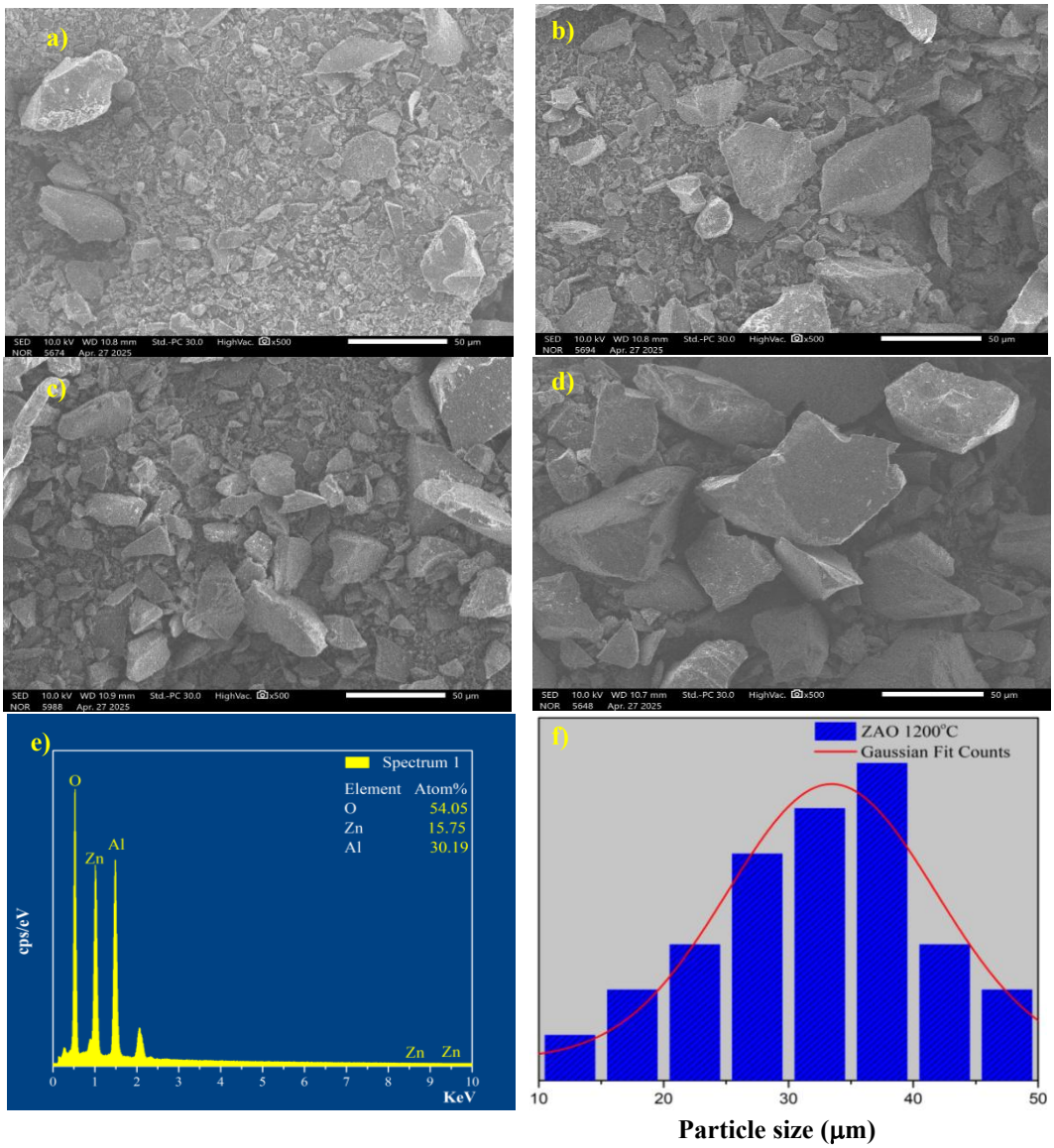

Figure 5. SEM images of the $ZnAl_2O_4$: 0.5 mol% Mn^{4+} phosphors annealed at the various temperatures a) 900°C, b) 1000°C, c) 1100°C, d) 1200°C, e) the EDX spectrum, and f) size distribution of the $ZnAl_2O_4$: 0.5 mol% Mn^{4+} powder annealed at 1200°C

3.4. Raman analysis

Figure 6 shows the Raman spectra of $ZnAl_2O_4$: 0.5 mol% Mn^{4+} powders annealed at various temperatures. Raman spectroscopy has been used to investigate alterations in the local structure of $ZnAl_2O_4$ crystals with different fuels. The Raman spectra of the four samples are presented in Figure 6. Based on group theory,

spinel's structure exhibits 42 normal vibrational modes at the Brillouin zone center, comprising three acoustic modes and 39 optical modes. As expressed in the following equation, these modes can be classified into symmetry species (Rodrigues et al., 2020).

$$T = A_{1g}(R) + E_g(R) + T_{1g}(R) + 3T_{2g}(R) + 2A_{2u} + 2E_u + 4T_{1u}(IR) + 2T_{2u} \quad (2)$$

Where Raman-active is R, infrared-active, and the remaining are silent (IR). The E_u, E_g, and T_{1g}, T2g, T_{1u}, T_{2u} modes are doubly and triply degenerate, respectively. Five Raman active A1g, E_g, $^3T_{2g}$ are observed in the case of spinel structures.

The Raman pattern of the samples annealed at 900°C, 1000°C, 1100°C, and 1200°C exhibits distinct characteristic peaks at 420 cm^{-1} and 661 cm^{-1}, corresponding to E_g and T_{2g} modes, respectively. These are the signature modes of the spinel structure of $ZnAl_2O_4$. According to the previous report, the Raman spectra of the gahnite structure have five active modes. A_g, E_g, T_{2g}, located at 758 cm^{-1}, 418 cm^{-1}, and 659 cm^{-1}, respectively, reported in scientific works (Chopelas & Hofmeister, 1991; López et al., 2009). The analysis revealed a progressive sharpening of the diffraction peaks and a marked increase in intensity as the annealing temperature increased from 900 to 1200°C, indicating improved crystallinity at elevated temperatures. This result resembles the previously reported results (Jain et al., 2020; Rodrigues et al., 2020).

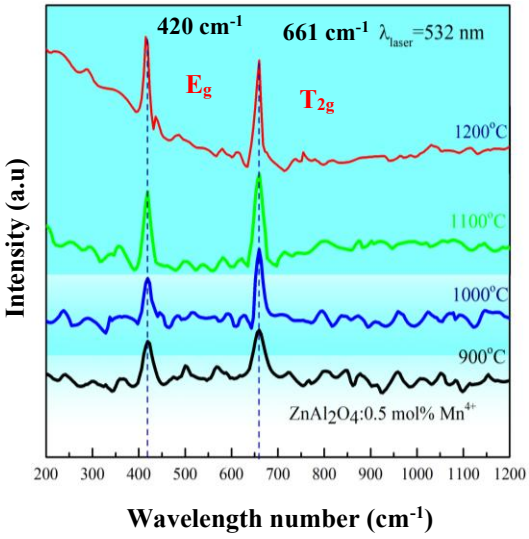

Figure 6. Raman spectra of $ZnAl_2O_4$: 0.5 mol% Mn^{4+} powders annealed at 900°C to 1200°C

3.5. Photoluminescence spectra

Figure 7a shows the photoluminescence spectra of $ZnAl_2O_4$: Mn^{4+} at various excitation wavelengths. The emission intensity varies significantly with different excitation wavelengths. Specifically, as the excitation wavelength increases from 395 nm to 458 nm and 535 nm, the sample's PL intensity tends to decrease. The PL spectrum features three distinct emission peaks: two firm, sharp peaks at 676 nm and 692 nm, and a weaker peak at 685 nm. It should be noted that the red emission originates from Mn^{4+} ions incorporated into the $ZnAl_2O_4$ host lattice, where Mn^{4+} ions preferentially substitute for Al^{3+} ions at the octahedral sites of the spinel structure. This substitution is facilitated by the similar ionic radii of Mn^{4+} (0.53 Å) and Al^{3+} (0.535 Å), which allows Mn^{4+} ions to occupy the Al^{3+} lattice positions with minimal structural distortion. The spinel lattice provides a highly symmetrical crystal field environment that significantly influences the electronic structure of Mn^{4+}. Under this crystal field, the d-orbital energy levels of Mn^{4+} are split, enabling radiative electronic transitions, particularly the $^2E_g \rightarrow {}^4A_{2g}$ transition, which is responsible for the characteristic red emission. Furthermore, the interaction between Mn^{4+} ions and the surrounding crystal lattice—through crystal field strength and local coordination—plays a crucial role in determining both the spectral position and the intensity of the observed emission. (Do et al., 2020). Based on the PL intensity shown in Figure 7, this study identifies 395 nm as the optimal excitation wavelength for maximising luminescence.

Figure 8 describes the PL spectra of $ZnAl_2O_4$: 0.5 mol% Mn^{4+} phosphors annealed at different temperatures for 4 hours in the air under an excitation wavelength of 395 nm, which indicates two emission peaks at 676 and 692 nm in the wide band 660 - 720 nm. The electron energy transfer from ^2E_g to $^4A_{2g}$ in Mn^{4+} ions could explain the red emission band. It is noted that the emission intensity increases with increasing annealing temperature from 900 - 1200°C and reaches a maximum of 1200°C. Thus, the optimal annealing temperature of $ZnAl_2O_4$: 0.5 mol% Mn^{4+} is 1200°C.

Figure 9 presents the photoluminescence (PL) spectra of $ZnAl_2O_4$:x mol% Mn^{4+} (x = 0.3–0.9 mol%) phosphors annealed in air at different temperatures for 4 h under excitation at 395 nm. The PL spectra exhibit two prominent emission peaks at approximately 676 and 692 nm, which correspond to the characteristic red emission of Mn^{4+}-doped $ZnAl_2O_4$. These emissions are attributed to the electronic transitions of Mn^{4+} ions incorporated into the $ZnAl_2O_4$ host lattice. In addition, the emission intensity increases with increasing Mn^{4+} concentration from 0.3 to 0.5 mol%, reaching a maximum at 0.5 mol%, after which it decreases. However, the emission intensity tends to reduce at higher doping concentration. Therefore, the best concentration for doping Mn^{4+} ions into $ZnAl_2O_4$ host lattice is 0.5 mol%, annealed at 1200°C.

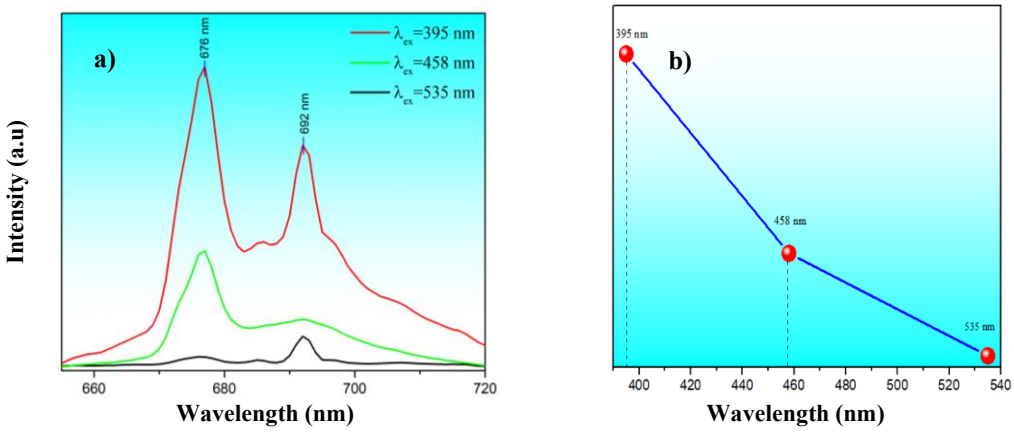

Figure 7. a) The PL spectrum of $ZnAl_2O_4$: Mn^{4+} at various excited wavelengths, and b) dependence of the PL intensity on the excited wavelength

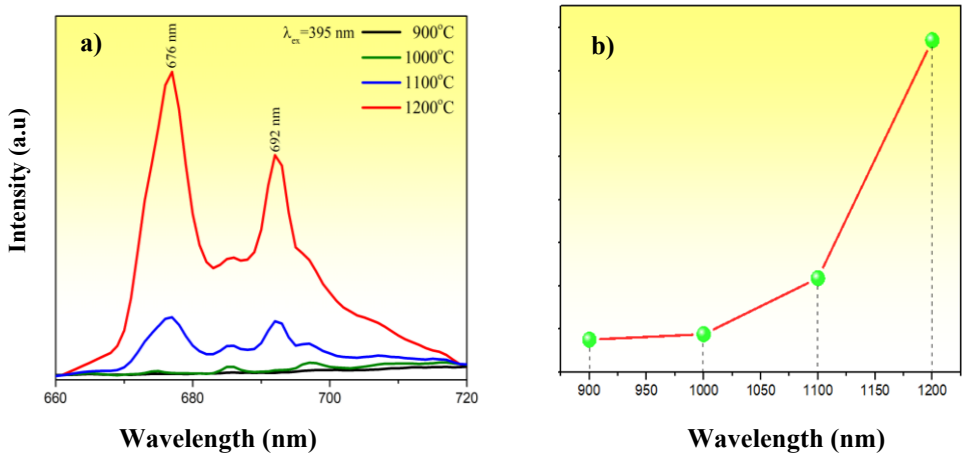

Figure 8. a) Shows the PL spectra under an excitation wavelength of 395 nm from $ZnAl_2O_4$: Mn^{4+} powder annealed at different temperatures for 4 hours, and b) dependence of the PL intensity on the annealing temperature

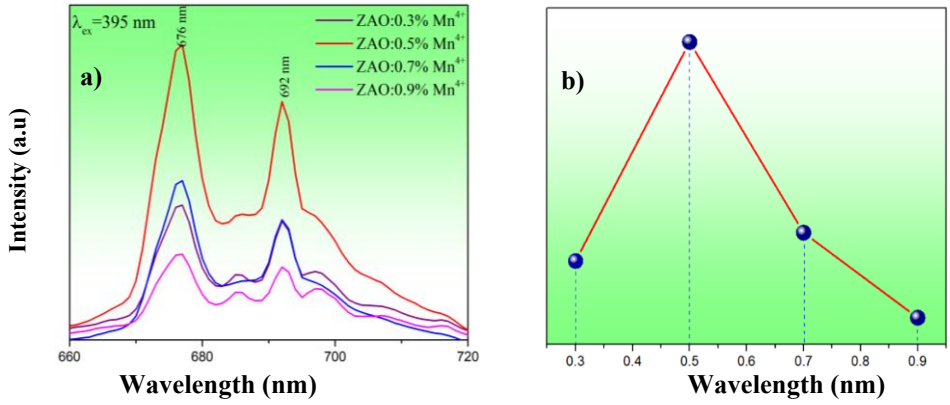

Figure 9. a) Shows the PL spectra under an excitation wavelength of 395 nm from $ZnAl_2O_4$: x mol% Mn^{4+} phosphors (x = 0.3, 0.5, 0.7, 0.9 mol%) annealed at 1200°C for 4 hours, and b) dependence of the PL intensity on the concentration for doping Mn^{4+} ions

3.6. Colorimetric properties

Figure 10 shows that the CIE chromaticity coordinates are used to evaluate the emission performance of $ZnAl_2O_4$: 0.5 mol% Mn^{4+} phosphor annealed at 1200°C for 4 hours in the air. The CIE chromatic coordinates for this sample shift from the yellow region to the white area, as shown in Figure 10. The calculated colour coordinates of the $ZnAl_2O_4$: 0.5 mol% Mn^{4+} phosphor could be derived from CIE 1931 directly, and the results indicate that the $ZnAl_2O_4$: 0.5 mol% Mn^{4+} phosphor locates in the white region with colour coordinates of (x, y) = (0.2705, 0.2741).

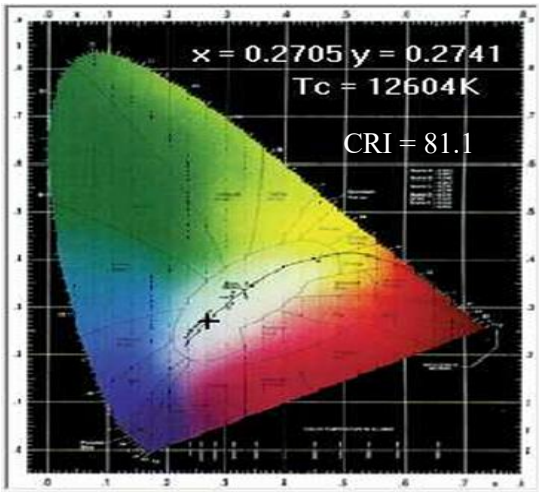

Figure 10. The CIE chromatic coordinates diagram of $ZnAl_2O_4$: 0.5 mol% Mn^{4+}

In contrast, the $ZnAl_2O_4$:0.5 mol% Mn^{4+} phosphor annealed at 1200°C exhibited a high correlated colour temperature (CCT) of 12604 K and a colour rendering index (CRI) of 81.1. Typically, commercial phosphors used in lighting applications have CRI values of 70–80, which are generally considered acceptable for general illumination. Therefore, the obtained CRI value of 81.1 slightly exceeds this conventional range, indicating that the material possesses suitable colour-rendering capability and is a promising candidate for white light-emitting diode (WLED) applications.

4. CONCLUSION

The sol-gel method successfully synthesised the red-emitting $ZnAl_2O_4$: 0.5 mol% Mn^{4+} phosphors. The analysis results show that the material has an average particle size of 10-50 µm, red emissions with two distinct peaks at 676 and 692 nm in the broad region 660 - 720 nm, and the highest intensity at 676 nm. The optimal Mn^{4+} doping concentration and the annealing temperature for the highest photoluminescence emission intensity are 0.5 mol% and 1200°C, respectively - the (x, y) CIE coordinates of (0.2705, 0.2741). The study results indicate that $ZnAl_2O_4$:0.5 mol% Mn^{4+} phosphors have potential applications in solid-state lighting LED devices.

CONFLICTS OF INTEREST

The authors report no financial or any other conflicts of interest in this work.

REFERENCES

Balakrishnan, S., Tiwari, A., Iyer, S., Kumbhar, P., Pusdekar, A., Ugemuge, N., & Muley, A. (2024). Energy transfer from Ce^{3+} to Eu^{3+} in the spinel structure of $ZnAl_2O_4$ phosphor for optoelectronic applications. *Radiation Effects and Defects in Solids*, *179*(5-6), 799-810. https://doi.org/10.1080/10420150.2024.2311820

Chopelas, A. M. H. A., & Hofmeister, A. M. (1991). Vibrational spectroscopy of aluminate spinels at 1 atm and of $MgAl_2O_4$ to over 200 kbar. *Physics and Chemistry of Minerals*, *18*, 279-293. https://doi.org/10.1007/BF00200186

Cornu, L., Duttine, M., Gaudon, M., & Jubera, V. (2014). Luminescence switch of Mn-Doped $ZnAl_2O_4$ powder with temperature. *Journal of Materials Chemistry C*, *2*(44), 9512-9522. https://doi.org/10.1039/C4TC01425A

Di Quarto, F., Zaffora, A., Di Franco, F., & Santamaria, M. (2023). Modeling of optical band-gap values of mixed oxides having spinel structure AB_2O_4 (A= Mg, Zn and B= Al, Ga) by a semiempirical approach. *ACS Organic & Inorganic Au*, *4*(1), 120-134. https://doi.org/10.1021/acsorginorgau.3c00030

Do, Q. T., Nguyen, T., Nguyen, V. Q., Tran, M. T., Nguyen, V. D., & Pham, T. H. (2020). Non-rare-earth dual green and red-emitting Mn-doped $ZnAl_2O_4$ phosphors for potential application in plan-growth LEDs. *Journal of Alloys and Compounds*, *845*, 156326. http://dx.doi.org/10.1016/j.jallcom.2020.156326

Trung, Q. D., Tu, N., Quang, V. N., Trung, M. T., Du V. N., & Huy, T. P. (2020). Non-rare-earth dual green and red-emitting Mn-doped $ZnAl_2O_4$ phosphors for potential application in plan-growth LEDs. *Journal of Alloys and Compounds*, *845*, 156326. http://dx.doi.org/10.1016/j.jallcom.2020.156326

Elliott, C., & Lee, K. (2020). Adoption of light-emitting diodes in common lighting applications (No. DOE/EE-2120). Guidehouse, Inc., Washington, DC (United States). https://doi.org/10.2172/1669047

Guilhaume, N., & Primet, M. (1994). Catalytic combustion of methane: copper oxide supported on high-specific-area spinels synthesized by a sol–gel process. *Journal of the Chemical Society, Faraday Transactions*, *90*(11), 1541-1545. https://doi.org/10.1039/FT9949001541

He, C., Ji, H., Huang, Z., Zhang, X., Fang, M., Wu, X., & Min, X. (2018). Preparation, structure, luminescence properties of europium doped zinc spinel structure green-emitting phosphor $ZnAl_2O_4$: Eu^{2+}. *Journal of Rare Earths*, *36*(9), 931-938. https://doi.org/10.1016/j.jre.2018.01.018

Jain, M., Manju, Kumar, R., Won, S. O., Chae, K. H., Vij, A., & Thakur, A. (2020). Defect states and kinetic parameter analysis of $ZnAl_2O_4$ nanocrystals by X-ray photoelectron spectroscopy and thermoluminescence. *Scientific reports*, *10*(1), 385. https://doi.org/10.1038/s41598-019-57227-8

Jiang, L., Zhang, X., Tang, H., Zhu, S., Li, Q., Zhang, W., ... & Liu, X. (2018). A Mg^{2+}-Ge^{4+} substituting strategy for optimizing color rendering index and luminescence of YAG: Ce^{3+} phosphors for white LEDs. Materials Research Bulletin, 98, 180-186. https://doi.org/10.1016/j.materresbull.2017.10.019

John, M. S., & John, F. (2023). Structural and morphological studies of optically active spinel structured nanocrystalline $ZnAl_2O_4$ synthesized by modified auto-ignition combustion method. *Journal of Materials Science: Materials in Electronics*, *34*(3), 178. https://doi.org/10.1007/s10854-022-09397-x

Khan, N., & Abas, N. (2011). Comparative study of energy saving light sources. *Renewable and sustainable energy reviews*, 15(1), 296-309. https://doi.org/10.1016/j.rser.2010.07.072

Kumar, K., Ramamoorthy, K., Koinkar, P. M., Chandramohan, R., & Sankaranarayanan, K. (2007). A novel way of modifying nano grain size by solution concentration in the growth of $ZnAl_2O_4$ thin films. *Journal of Nanoparticle Research*, *9*, 331-335. https://doi.org/10.1007/s11051-006-9108-3

Li, X., Zhang, C., Chen, J., Liu, Q., Bai, Z., Liu, X., & Mi, X. (2023). Cr^{3+} ions improving the spectral properties of YAG: Ce^{3+} luminescent ceramics for white LD lighting. *Ceramics International*, 49(3), 5489-5495. https://doi.org/10.1016/j.ceramint.2022.10.072

Liu, L., Keoleian, G. A., & Lewis, G. M. (2024). Life cycle cost analysis of LED retrofit and luminaire replacements for four-foot T8 troffers. *Lighting Research & Technology, 56*(4), 403-420. https://doi.org/10.1177/14771535231207810

López, S., Romero, A. H., Rodríguez-Hernández, P., & Munoz, A. (2009). First-principles study of the high-pressure phase transition in $ZnAl_2O_4$ and $ZnGa_2O_4$: From cubic spinel to orthorhombic post-spinel structures. *Physical Review B—Condensed Matter and Materials Physics*, *79*(21), 214103. https://doi.org/10.1103/PhysRevB.79.214103

Rodrigues, J., Hoppe, M., Sedrine, N. B., Wolff, N., Duppel, V., Kienle, L., ... & Monteiro, T. (2020). $ZnAl_2O_4$ decorated Al-doped ZnO tetrapodal 3D networks: microstructure, Raman and detailed temperature dependent photoluminescence analysis. *Nanoscale Advances*, *2*(5), 2114-2126. https://doi.org/10.1039/C9NA00730J

Ma, Y., Zhang, L., Zhou, T., Sun, B., Wang, Y., Kang, J., ... & Chen, H. (2020). High recorded color rendering index in single Ce, (Pr, Mn): YAG transparent ceramics for high-power white LEDs/LDs. *Journal of Materials Chemistry C*, *8*(13), 4329-4337. https://doi.org/10.1039/D0TC00032A

Martins, R. F., & Serra, O. A. (2010). Thin film of $ZnAl_2O_4$: Eu^{3+} synthesized by a non-alkoxide precursor sol-gel method. *Journal of the Brazilian Chemical Society*, 21, 1395-1398. https://doi.org/10.1590/S0103-50532010000700028

Mekprasart, W., Boonyarattanakalin, K., Pecharapa, W., & Ishihara, K. N. (2018). Optical characteristics of samarium doped $ZnAl_2O_4$ nanomaterials synthesized by vibrational milling process. *Materials Today: Proceedings*, *5*(6), 14126-14130. https://doi.org/10.1016/j.matpr.2018.02.076

Nuryadin, B. W., Sawitri, A., Mahen, E. C. S., & Nuryantini, A. Y. (2017, February). Synthesis and Morphology Properties of Mn-doped Zinc Aluminate ($ZnAl_{2-x}O_4$: xMn^{4+}, x = 1%) Using Co-Precipitation Methods with Microwave Thermal Assisted. In *Journal of Physics: Conference Series* (Vol. 812, No. 1, p. 012020). IOP Publishing. https://doi 10.1088/1742-6596/812/1/012020

Priya, R., Kaur, S., Sharma, U., Pandey, O. P., & Dhoble, S. J. (2020). A review on recent progress in rare earth and transition metals activated SrY_2O_4 phosphors. *Journal of Materials Science: Materials in Electronics*, 31, 13011-13027. https://doi.org/10.1007/s10854-020-03930-6

Vikas, Lahariya, V., Yadav, R., Tamrakar, R. K., Yadav, A., Gupta, G., & Dawar, A. (2023). Efficient deep-red luminescence with high colour purity from Mn^{4+}-doped $ZnAl_2O_4$ nanophosphor. *Journal of Materials Science*, *58*(37), 14645-14660. https://doi.org/10.1007/s10853-023-08920-7

Vikas, Lahariya, V., Tamrakar, R. K., & Butolia, S. (2025). Thermoluminescence glow curve study of UV-irradiated Mn^{4+} doped zinc aluminate spinel nanophosphor. *Journal of Materials Science: Materials in Electronics*, *36*(2), 171. https://doi.org/10.1007/s10854-025-14229-9

Wu, Y., Du, J., Choy, K. L., Hench, L. L., & Guo, J. (2005). Formation of interconnected microstructural $ZnAl_2O_4$ films prepared by sol–gel method. *Thin Solid Films*, *472*(1-2), 150-156. https://doi.org/10.1016/j.tsf.2004.07.084

Yadav, P. J., & Mahavidyalaya, K. N. (2018). Phosphor converted white led with improved CRI. *Journal of Applied Mathematics and Physics*, *6*(04), 657. https://doi.org/10.4236/jamp.2018.64058

Zhang, D., Wang, C., Liu, Y., Shi, Q., Wang, W., & Zhai, Y. (2012). Green and red photoluminescence from $ZnAl_2O_4$: Mn phosphors prepared by sol–gel method. *Journal of luminescence*, *132*(6), 1529-1531. https://doi.org/10.1016/j.jlumin.2012.01.025

Zhang, D., Guo, Q., Ren, Y., Wang, C., Shi, Q., Wang, Q., ... & Fan, Q. (2018). Influence of inversion defects and Cr–Cr pairs on the photoluminescent performance of $ZnAl_2O_4$ crystals. *Journal of Sol-Gel Science and Technology*, *85*, 121-131. https://doi.org/10.1007/s10971-017-4527-4

Zhu, B., Ren, S., Zhang, D., Wang, Q., Yang, B., Wang, Q., ... & Liu, C. (2021). Tuning structural and optical characteristics with Mn^{2+} introduced into $ZnAl_2O_4$: Cr^{3+} nanophosphors: energy transfer process and cations rearrangement. *Journal of Luminescence*, 239, 118362. https://doi.org/10.1016/j.jlumin.2021.118362